International Journal of Solids and Structures 51 (2014) 2840–2849

Contents lists available at ScienceDirect

International Journal of Solids and Structures

journal homepage: www.elsevier.com/locate/ijsolstr

Suppression of necking in incremental sheet forming

D.Y. Seong [a,1], M.Z. Haque [a], J.B. Kim [b], T.B. Stoughton [c], J.W. Yoon [d,*]

[a] Faculty of Engineering and Industrial Sciences, Swinburne University of Technology, Melbourne, VIC 3122, Australia
[b] Dept. of Mechanical and Automotive Eng., Seoul National Univ. of Tech., Seoul 139-743, Republic of Korea
[c] General Motors Global Research and Development Center, MC 480-106-244, Warren, MI 48090-9055, USA
[d] School of Engineering & Institute for Frontier Materials, Deakin University, Geelong Waurn Ponds, VIC 3220, Australia

ARTICLE INFO

Article history:
Received 17 July 2013
Received in revised form 20 January 2014
Available online 13 April 2014

Keywords:
Incremental sheet forming (ISF)
Stress gradient
Stress-based forming limit
Necking

ABSTRACT

Incremental sheet forming enables sheet metal to deform above a conventional strain-based forming limit. The mechanics reason has not been clearly explained yet. In this work, the stress-based forming limit was utilized for through-thickness necking analysis to explain this uncovered question. Stress-based forming limit which has path-independency shows that the stress states in top, middle and bottom surfaces did not exceed the forming limit curve at the same time and each layer has different stress state in terms of their deformation history to suppress necking. It has been found that it is important to consider the gradient stress profile following the deformation history for the proper forming limit analysis of incremental sheet forming.

1. Introduction

Incremental sheet forming (ISF) is being popularly used to form a complicated shape beyond the formability of a sheet material as an innovative forming technology. However, it has been difficult to find a sound mechanics reason why incremental sheet forming can suppress (or delay) necking and how to stabilize the deformation of a sheet material.

In mechanics viewpoint, incremental sheet forming example in this manuscript is a clamped plate under dynamic point loading. Bending of a thick or thin clamped plate under elastic loading can be found in the pioneering works done by Hencky (1913), Galerkin (1915), Love (1927), Timoshenko and Krieger (1959). Footnote to page 197 of Timoshenko and Krieger (1959) gives a detailed explanation of history of plates under bending. Also, an analytical work by Love (1927) explains the tensile deformation of under bending with curvilinear & polar coordinate system which is similar to the mechanics of incremental sheet forming.

A review paper related to incremental sheet forming discussed six new mechanisms such as contact stress, bending under tension, shear effect, cyclic loading effect, geometrical inability, and hydrostatic pressure which lead to preventing unstable deformation from the viewpoint of a necking (Emmens and van den Boogaard, 2009).

Most of developments for incremental sheet forming have utilized a conventional forming limit in the strain space. Necking limit in the strain space is dependent on anisotropic yield functions and their material parameters (Dasappa et al., 2012). In addition, several theoretical studies showed that the strain-based forming limit using MK (Marciniak–Kuczynski) necking theory is also strongly dependent on the strain path (Stoughton, 2000; Stoughton and Yoon, 2005; Stoughton and Zhu, 2004). Although a deformation history mainly depends on tool path in ISF, the path-dependent forming limit has been being used to estimate necking.

The concept of path-independent forming limit such as stress-based forming limit was introduced for a valid necking assessment irrespective of a changing loading scenario. This stress-based limit curve in the plane-stress condition is extended to the forming limit in three-dimensional loading using equivalent stress and mean stress space (Simha et al., 2007). In addition, it was experimentally observed that any necking didn't occur during pure bending (Tharrett and Stoughton, 2003), because of the compressive stress in the concave part which made the stress state below the limit and prevented a through-thickness necking instability (Stoughton and Yoon, 2011). A recent ISF simulation found a stress combination of strong bending and membrane tension in some sheet elements (Guzmán et al., 2012).

In this work, the path-independent stress-based forming limit was utilized taking into account stress-gradient histories through the thickness direction in order to explain more scientific

* Corresponding author at: School of Engineering & Institute for Frontier Materials, Deakin University, Geelong Waurn Ponds, VIC 3220, Australia. Tel.: +61 3 5227 3425.
E-mail address: j.yoon@deakin.edu.au (J.W. Yoon).
[1] Current Address: LG Production Engineering Research Institute, LG Electronics, Cheongho-Ri, Pyungtak-City, Kyoungki-Do, Republic of Korea

http://dx.doi.org/10.1016/j.ijsolstr.2014.04.007
0020-7683/

explanation why the incremental sheet forming prevents a neck from initiating and activating.

2. Role of stress and strain gradient to necking

One of the primary factors that cause confusion in understanding forming limits is the role of the stress and strain gradients through the sheet thickness. These gradients are intrinsic to curved sheet and therefore critical to understanding and applying forming limit criterion based on stress or strain. For example, stretching a 1 mm thick sheet over a 2 mm radius will introduce a difference in the true strain between the top and bottom side of the sheet of up to $ln(1.5) = 0.405$, depending on the amount of in-plane tension that thins the metal. That strain difference is on the order of the FLDo value of most steels and twice the limit of aluminum. So this raises the question, "What layer do you use to define the stress (or strain) that will be compared the stress (or strain FLC) in the formability analysis?" When industry first started to implement the FLD in the 1960's, it was quickly discovered that strains measured most conveniently on the convex side of the sheet were commonly found to be well above the FLC with no sign of necking. Remarkably, without any experimental evidence to justify the decision, the metal forming industry adopted the approach of using the membrane strains in making comparison to the strain FLC. This assumption has continued unchecked in both physical tryout and analysis of numerical simulations for nearly two decades, and continues to be the dominant practice used in industry today, more than four decades later. Unfortunately, the assumption is wrong, and the truth has serious consequences in both the interpretation of forming limits and their application in analysis.

Tharrett at General Motors conducted a series of simple bending under tension tests on strips of different thickness of steel, aluminum, and brass and different punch tip radii with the objective to determine what strains through the thickness are the cause of necking. He discovered that necking initiated not when the membrane strains exceeded the strain FLC, as was previously thought, but much later in the forming process, when the strains on the concave side of the sheet rose to the level of the FLC. While the tests were limited to plane strain conditions, the results were confirmed in all materials and tooling geometry. The details of the experiments for steel were later published by Tharrett and Stoughton (2003), and the results for one test geometry are shown in Fig. 1. There are two necks observed in this specimen on either side of the center punch tip radius at the location where the strains on the concave side, shown by the enlarged circles, rose to the level of the FLC for this material.

Considering the importance of stress metrics, Stoughton and Yoon (2011) noted that Tharrett's results are also understood to apply to the stress conditions, so that this important factor can be applied to both linear and nonlinear deformation processes. In other words, for a neck to initiate, the stress on all layers through the thickness must exceed the stress FLC. To put this idea into practice in numerical simulation, the forming limit criterion must be applied to each integration point through the thickness of the element. In other words, necking is defined to initiate only when the formability index is larger than 1 at all integration points. This generalization has interesting consequences because often the stress field is more complex than the strain field, due for example, to a history of cycling bending/unbending. So the minimum or least critical layer may not be on the surface, but at an interior integration point. Furthermore, it is important to note that use of membrane values, which is the most widely accepted practice for formability assessment by industry, will result in overly conservative predictions of necking on curved sheet. This mistake will undermine correlation with experiment, but also, because the level of the conservative estimate is proportional to the strain gradient through the thickness, it will result in a proportional bias in the safety margin towards regions of higher curvature, while providing no additional margin of safety in regions of zero curvature or through-thickness stress gradient. Since failures most often occur away from curved areas of the product for this very reason, the bias of using membrane strains in formability assessment provides no real benefit to producing robust processes. Another interesting consequence of Tharrett's results is that it explains why necking is not often observed in hemming and never observed in pure

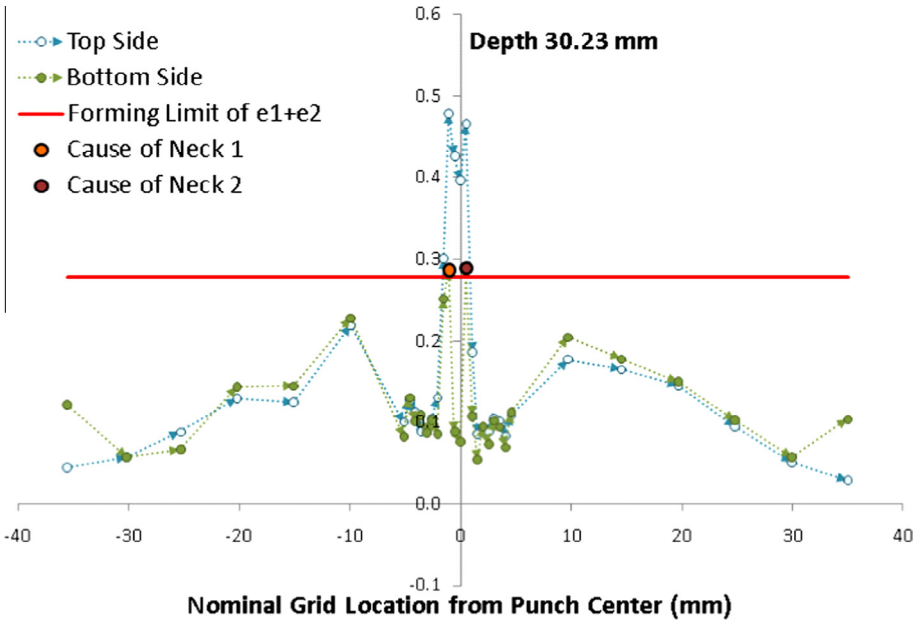

Fig. 1. Sum of the principal strains for a 50 wide strip of 1008 AK steel stretch-bent over a punch wedge with a ¼ inch radius to the depth at which onset of necking occurs, as reported (Tharrett and Stoughton, 2003). The forming limit is characterized as a simple limit on the sum of the principals because the minor strain was less than or equal to zero at all points along the strip in a region of the FLD characterized by a limit on thinning strain for this metal. The FLC and FLDo was obtained from standard FLD tests independent of the stretch-bend test.

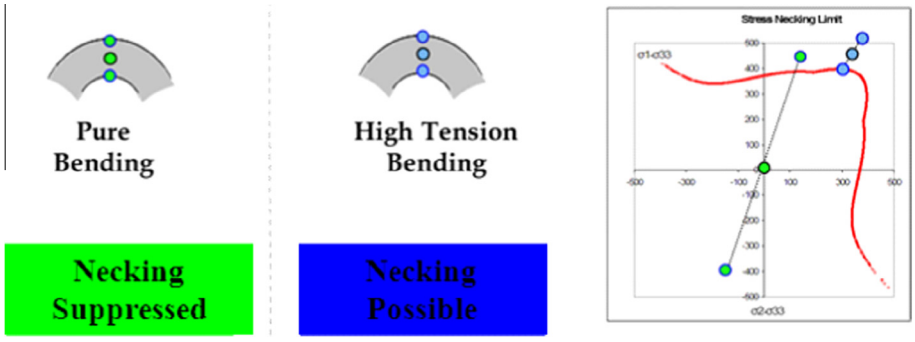

Fig. 2. Necking under pure bending and high tension bending (Stoughton and Yoon, 2011).

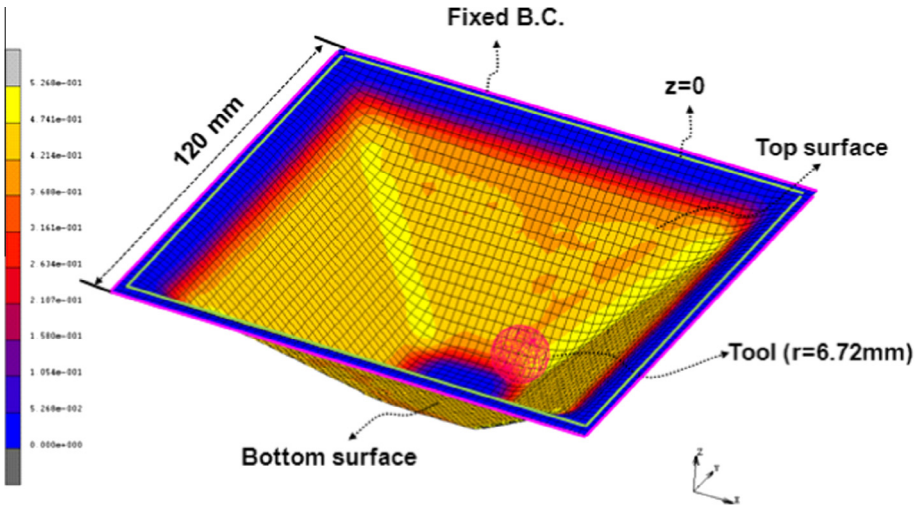

Fig. 3. Simulation of the ISF for a pyramidal-shaped part.

bending. Fig. 2 (Stoughton and Yoon, 2011) illustrates why the compressive stress on the concave side of the bend that occurs in pure bending does not allow the necking criteria to be satisfied. This explanation is applied to incremental sheet forming later in this work.

3. FE modeling of incremental sheet forming

The ISF (incremental sheet forming) for a pyramidal-shaped part was chosen for an example, because most of the pyramidal parts deform along the plane strain path. The plane strain path is the severest case from the viewpoint of the forming limit. The FEM simulations were carried out as shown in Fig. 3 where a commercial implicit FEM software called MSCMarc (MSC Software, 2010) was used with a thick shell formulation with reduced integration (the library number of 140). Five integration points were assigned through the thickness direction. Planar anisotropic material properties with a thickness of 1 mm, where Hill's 1948 yield function were used. The length and width of the initial elements are 2.5 mm × 2.5 mm. The dimension of the initial blank is 160 mm × 160 mm. In the initial FEM modelling, the rolling direction is coincided with the global X-direction. The fixed boundary condition was imposed on all edges of the blank as shown in Fig. 3. A ball-shaped tool with a radius of 6.72 mm was modelled as a rigid body. A contact condition between the tool and the blank is frictionless assuming well lubricated condition. A forming depth in each step is 0.5 mm. In this work, the Voce law was used for AA 6022-T4E32 material with Eq. (1) as the hardening function.

Table 1
Planar anisotropic material properties for the aluminum sheet of 6022-T4E32.

	A (MPa)	B (MPa)	C	r
Biaxial	355.91	221.48	6.977	1.244
0°	328.36	194.5	10.941	0.82
45°	325.9	192.76	9.175	0.418
90°	316.01	188.75	10.123	0.664

$$h(\bar{\varepsilon}^p) = A - B\exp(-C\bar{\varepsilon}^p) \quad (1)$$

All the planar anisotropic material properties are described in Table 1. All the coefficients for Hill's 1948 planar anisotropic yield function were determined based on three *r*-values (0, 45, 90 degrees from the rolling) and one stress-ratios (biaxial to rolling) shown in Table 1. The obtained coefficients are F = 1.3707, G = 1.1099, H = 0.9101, N = 2.2773. The biaxial curve is used as the reference curve for FE analysis.

Effective plastic strain contours were shown in Fig. 4. Obviously it is shown that effective strains in the middle layer are much lower than the ones on the top and bottom layers. It implies that top and bottom layers have experienced much more complex stress history than the middle layer. Especially, the stress at the top layer is more complex and dynamic due to the contact, which accumulates more plastic strain. The contact also effects on the stress-gradient though the thickness. Repeated bending/unbending behaviors increased the plastic strain on both the top and bottom layers. This will be discovered in the next section.

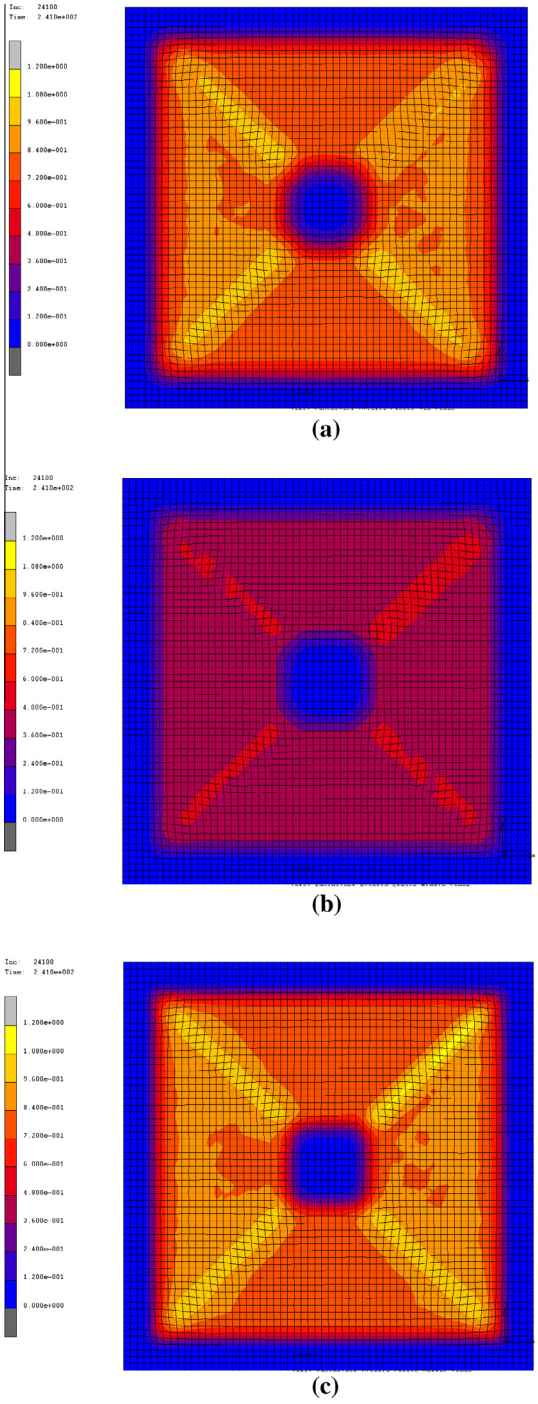

Fig. 4. Effective strain distributions in the top, middle, and bottom layers at the final stage: (a) top layer, (b) middle layer, and (c) bottom layer.

4. Necking analysis using the final values of stress and strain data

In order to model strain-based FLC, MK (Marciniak–Kuczynski) model is used as.

$$[1-D]\left[\frac{h(\bar{\varepsilon}^b)}{h(\bar{\varepsilon}^a)}\right]\left[\frac{\bar{\sigma}^b}{\bar{\sigma}^a}\right]=1 \tag{2}$$

where D is the value to characterize and quantify the thickness imperfection quantitatively. For typical commercial alloys, the studies of damage microscopic observations and probability calculations have shown that D is 0.4% (Hong et al., 2008). D = 0.004 is used in this work. The calculated FLC is displayed in Fig. 5(a) using a red line. Plastic strains at the final stage are also presented in the principal strain space. It was shown that the final values of the plastic strain calculated from integration points in the top, middle and bottom layers are above the necking limit. Most of plastic strain data are located between the plane strain and biaxial tension paths. The integration point on the top layer has a higher value of plastic strain than any other integration point, while the integration point on the bottom layer has a lower strain. The strain distribution is significantly changed through the sheet thickness.

In the strain-based FLC, it is assumed that deformation path is linear and proportional which means that the ratio of $(\rho = d\varepsilon_2/d\varepsilon_1, 0 \leqslant \rho \leqslant 1)$, the minor to major plastic strain increment, is always constant during the deformation. Stoughton and Yoon (2012) discussed that strain-based FLC cannot be used even for a linear path when pre-strain is developed. Incremental sheet forming shows an extreme violation for the use of a conventional forming limit due to complex deformation modes.

The principal strain ratio (ρ) in the Eq. (3) is converted into the principal stress ratio (α) in the Eq. (4).

$$\begin{bmatrix} e_1^{FLC} \\ e_2^{FLC} \end{bmatrix} = e_1^{FLC}\begin{bmatrix} 1 \\ \rho \end{bmatrix}^{(\text{strain-based FLC})} \tag{3}$$

$$\begin{bmatrix} \sigma_1^{FLC} \\ \sigma_2^{FLC} \end{bmatrix} = \sigma_1^{FLC}\begin{bmatrix} 1 \\ \alpha \end{bmatrix}^{(\text{strain-based FLC})} \tag{4}$$

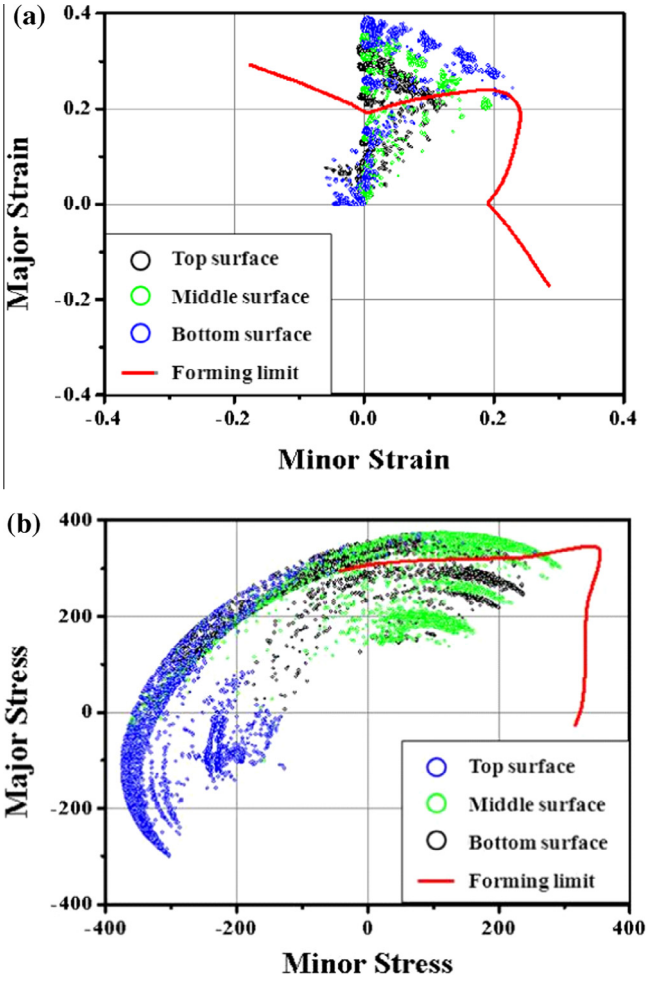

Fig. 5. Forming limit curves at the final stage: (a) strain-based FLC and (b) stress-based FLC.

Details to derive the Eq. (4) is described in the work of Stoughton and Yoon (Stoughton and Yoon, 2005). The stress-based FLC is described using α which is the ratio of the minor to major principal stresses. Stress-based forming limit is constructed in Fig. 5(b).

Because of the differences in stresses between continuous loading and unloading by the tool movement, therefore, a projection method based on the final stresses only was introduced to compensate the current unloaded stress by projecting it back to the current yield surface or hardening (called the projected stress) using the following equation (Stoughton and Yoon, 2011).

$$\sigma_{ij}^{p} = \sigma_{ij} \frac{h(\bar{\varepsilon}_p)}{\bar{\sigma}(\sigma_{ij})} \tag{5}$$

In the reconstruction, the projected stress is based on the effective plastic strain and the set of the final stress components. The projected stress state is determined by the effective plastic strain and yield function. The projected stresses calculated using the Eq. (5) are plotted for the stress-based forming limit curve as shown in Fig. 5(b).

Final stress data in top, middle, and bottom integration points of the sheet are above the forming limit. Positive values of the minor stress dominate in the bottom and middle layer, while compressive minor stress dominates on the top layer, which is due to unloading and springback. Obviously, necking should occur in both the strain-based FLC and the projected stress-based FLC when strains and stresses at the final state are used in the necking assessment.

In order to assess necking, the pyramidal part with an angle of 45° and a depth of 40 mm was fabricated using an ABB robot. Square grids with a length of 2.5 mm were marked on AA 6022-T4E32 sheet with 1 mm thickness. The laser milling machine was used for the grid marking with a width of 0.5 μ and a depth of 0.4 μ. The speed of ball-shaped tool is ensured to be 25 mm/s during the experiment, and the forming depth in each step is 0.5 mm. As shown in Fig. 6, necking or fracture was not observed in the fabricated pyramidal part using the ISF. Therefore, both results based on the final strain or stress data are not compatible with the experimental observation.

5. Necking analysis considering the deformation history

In this section, all the stress history is taken into consideration for the necking analysis. Based on the experimental FLC measured

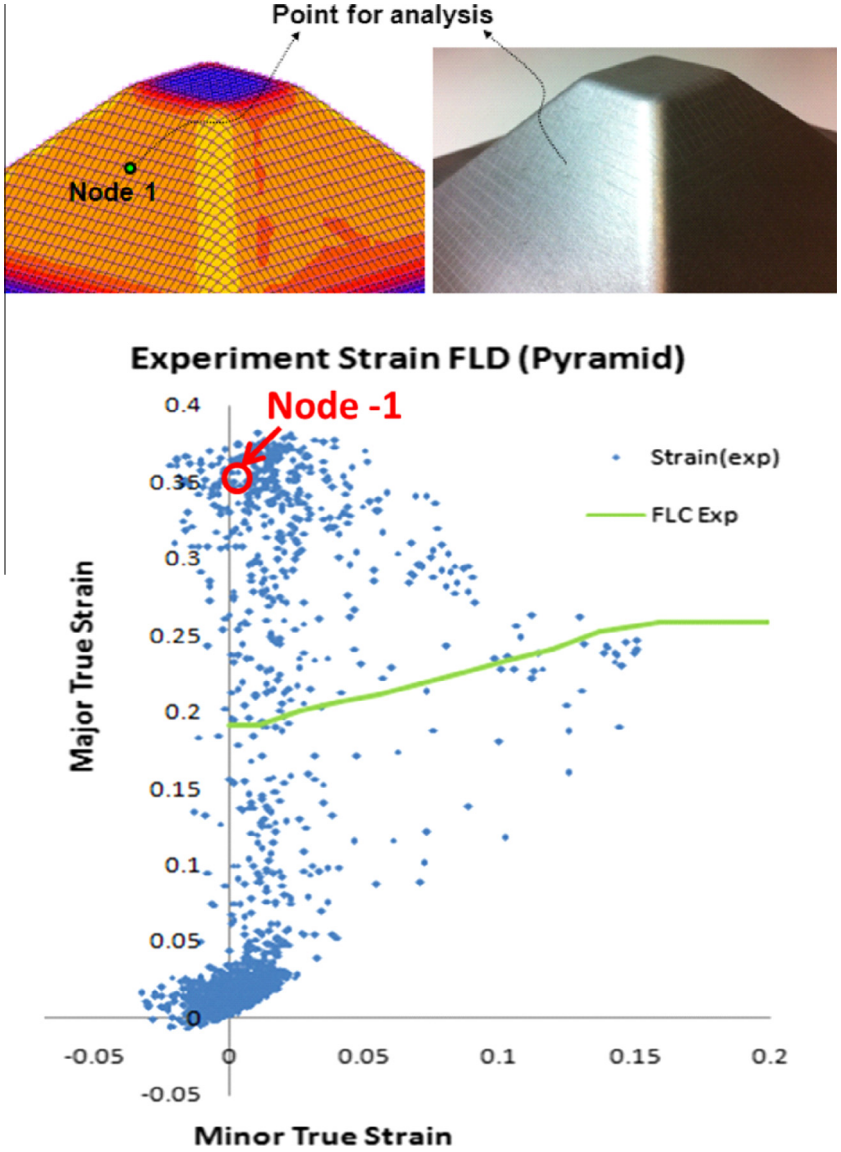

Fig. 6. Selection of Node-1 from Experimental FLC. The pyramidal part with an angle of 45° and a depth of 40 mm was compared. Strains were measured in square grids with a length of 2.5 mm. Node 1 was selected as one of the nodes deforming in the typical plain strain path.

from a pyramidal shape shown in Fig. 6, the node-1, which is located at a typical plane strain condition at the final state, is investigated for the sake of a clear understanding. At the node 1, the measured major strain from the experiment is 0.365, while the minor strain is almost zero. The strains were measured from the four neighbor elements around node 1, and then an average value is taken to compare it with the simulated result. In the simulation, major strain and minor strain in the top surface are 0.380 and 0.002, respectively. The experimental measurements rare compatible with the forming limit prediction in Fig. 5(a).

The plastic strain history at node 1 is illustrated as shown in Fig. 7, where stress and strain data in every time step are exported from the output file. Fig. 7(a) shows that the mid-surface nearly follows a plain-strain path. But, the cyclic deformation paths are observed between uniaxial and plane strain (for the top surface) and between biaxial and plane strain (for the bottom surface). These cyclic strain behaviors in the simulation of incremental sheet forming were also discussed in the work of Eyckens et al. (2007) .

Increasing ratios of the effective plastic strain on the top and bottom layers are almost twice than the one in the middle layer as shown in Fig. 7(b). It is important to know that the plastic strain occurs almost along the plane strain path, although the plastic strain increment are far from the plane strain path. Necking limit mainly depends on the principal strain ratio. Stoughton and Yoon (2012) showed that if the principal strain ratio changes during the deformation, the strain-based FLC is not valid anymore due to its sensitivity to the path. So, it is natural that the strain-based FLC cannot predict the necking behavior of incremental sheet forming.

On the other hand, the historical projected stresses at node 1 are presented in the stress-based forming limit as shown in Fig. 8. Three sections are defined in terms of the level of the

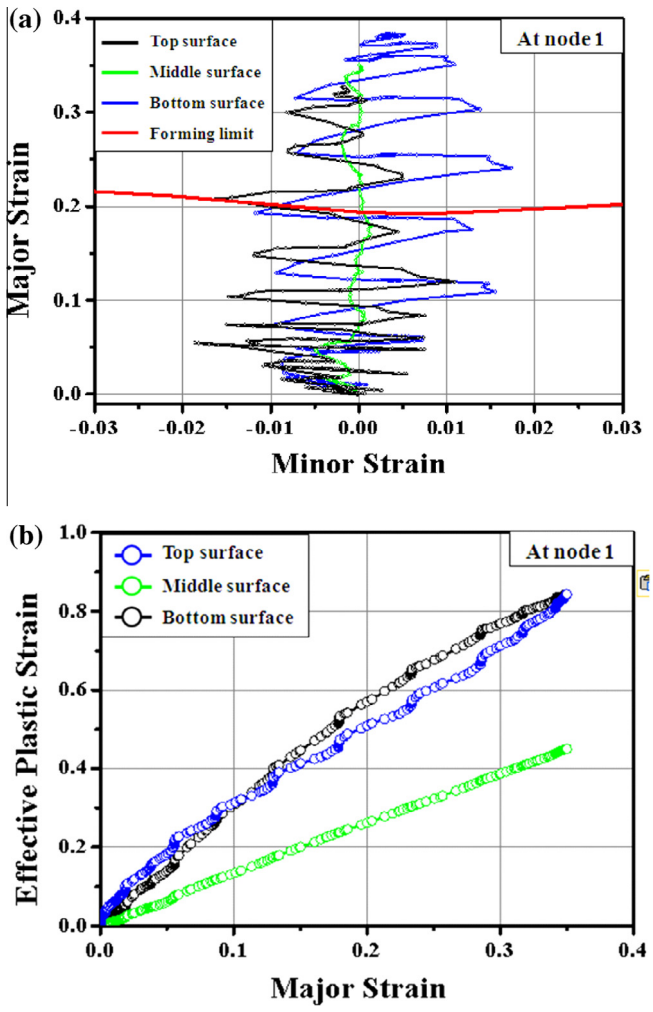

Fig. 7. Plastic strain history at node 1: (a) principal strain history and (b) effective plastic strain history.

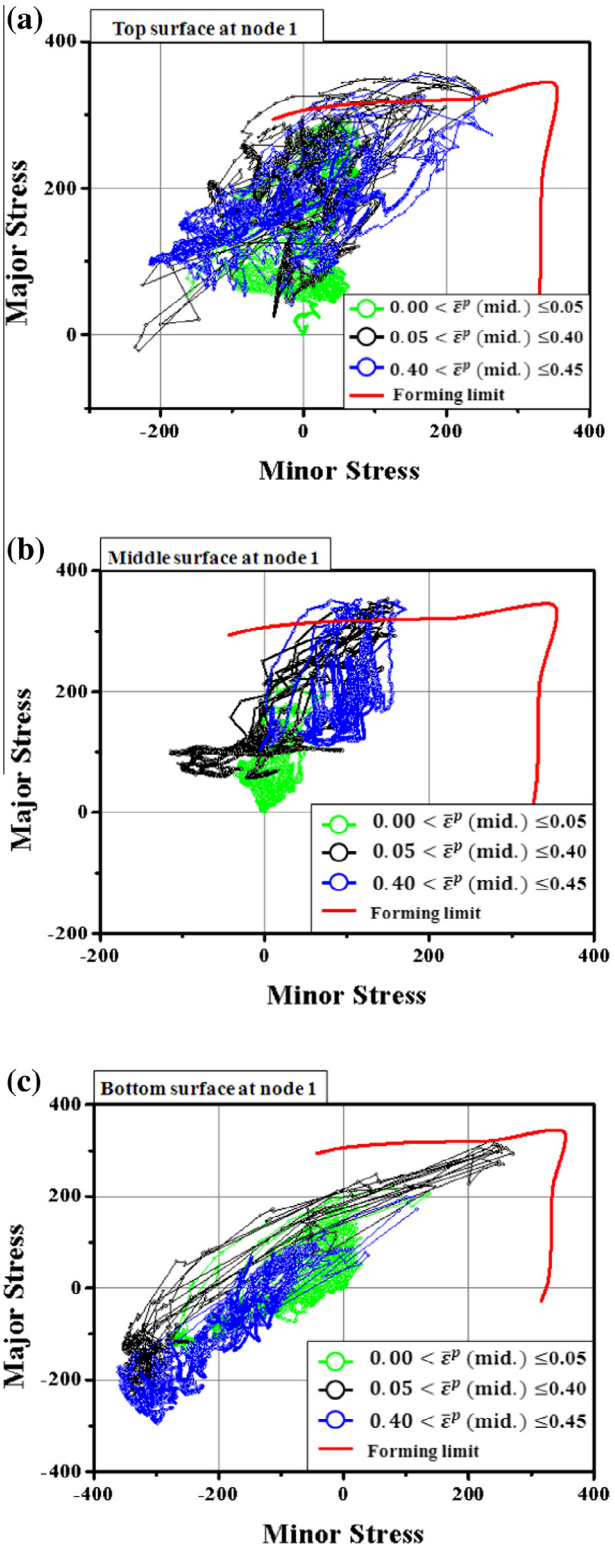

Fig. 8. Stress histories at node 1 for all layers: (a) top surface, (b) middle surface, and (c) bottom surface.

effective plastic strain in the middle layer; $0 < \bar{\varepsilon}_p \leq 0.05, 0.05 < \bar{\varepsilon}_p \leq 0.40$, and $0.40 < \bar{\varepsilon}_p \leq 0.45$. The stresses in bottom and middle layer are repeatedly above the forming limit, while the stress on the top layer is always below the limit. In this case, the material deforms without experiencing necking instability and the deformation does not reach necking yet (as shown in Fig. 2)

One of the interesting things is that the deformation mode on the top surface is different from the one on the bottom surface. The stress states on the top surface are bi-axial compression, plane strain, uniaxial and pure shear. The stress states on the bottom surface are mainly bi-axial tension and bi-axial compression. The deformation mode is obviously much more complex than just cyclic bending and unbending. However, the plane strain state in the major direction is dominated in the middle layer.

6. Suppression of necking by gradient strain and stress

In order to investigate the different deformation modes through the thickness direction, tool positions are defined as shown in Fig. 9. At the tool position A, the deformation at node-1 is elastic. The contact between node-1 and the tool occurs when the tool passes through the tool position B, while the tool position C is one of the tool locations during the contact. Springback starts again when the tool passes through the position D after the contact. Effective plastic strains in all layers increase between the tool positions, B and C as shown in Fig. 10(a).

Fig. 10(b) shows the strain histories of all the layers in terms of the tool positions during a single step of incremental tool path. Strain in the middle surface deforms along the plane strain path irrespective of the tool position. When the tool is moving from position A to position B or from position C to position D, the minor strain in the top surface decreases, while that on the bottom surface increases. When the tool is moving from the position B to C, the minor strain behaviors are opposite. The minor strain in the top surface increases, while that in the bottom surface decreases. It is interesting that the bottom surface has a positive value of a minor strain increment when the top surface has a negative value of a minor strain increment and vise versa. Although the ISF causes the cyclic strain behaviors both on the top and bottom surfaces, the direction of the minor strain is opposite each other.

In the stress space, stress changes abruptly with the sign change of the minor strain. The strain histories were converted into the stress space as shown in Fig. 11. The stresses in the bottom layer and the middle layer exceed the necking limit only when the tool is moving between tool positions of B and C. However, the stresses on the top surface are always below the limit. The stress in the middle layer is along the plane strain path. Just before contact to the tool, node 1 has the positive values of major stresses on the

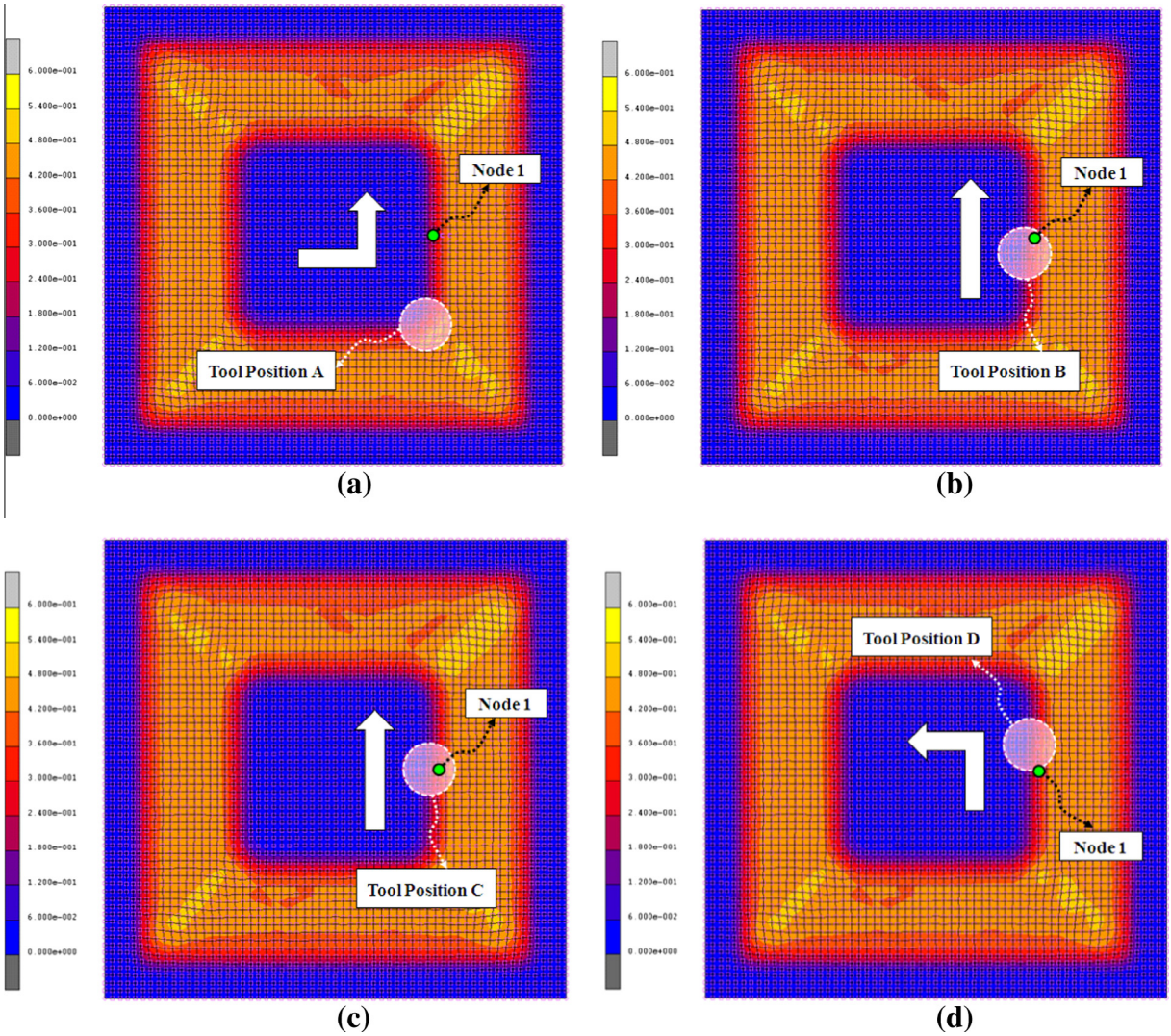

Fig. 9. Defined Tool Positions: (a) tool position A, (b) Tool Position B, (c) tool position C, and (d) tool position D.

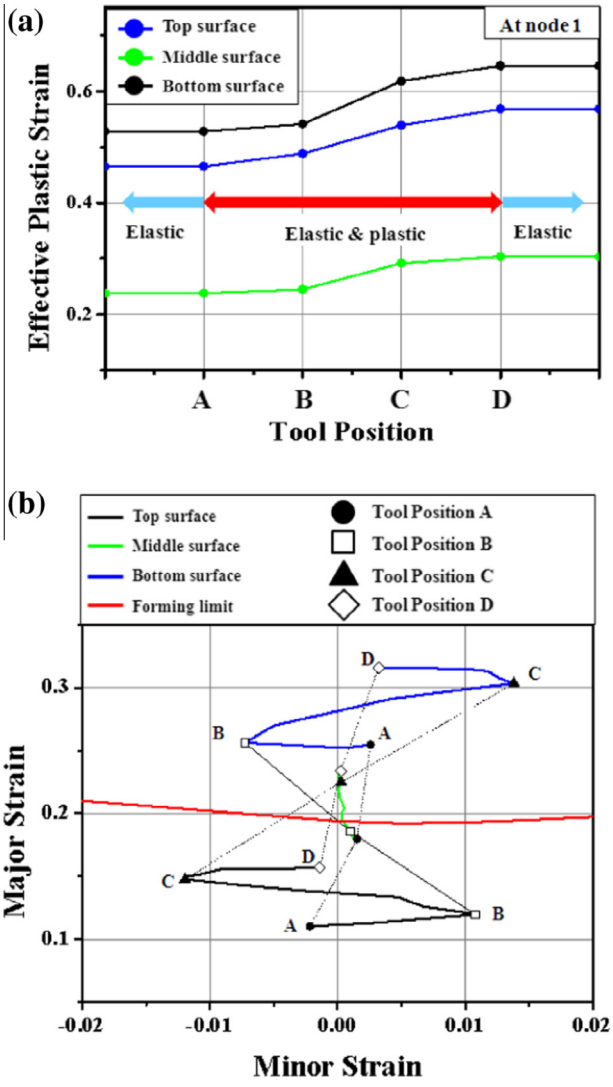

Fig. 10. Strain history at node 1 in terms of the defined tool positions: (a) effective strain history and (b) strain history.

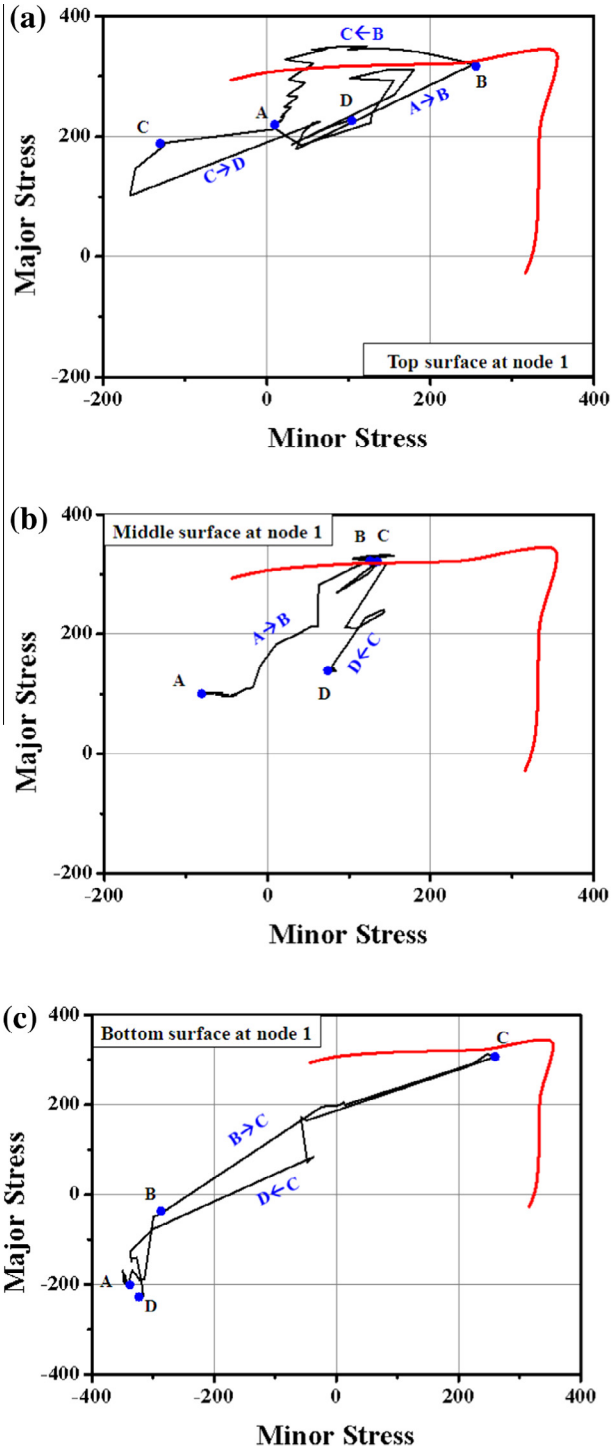

Fig. 11. Stress history at node 1 in terms of the defined tool positions: (a) stress in the top layer, (b) stress in the middle layer, and (c) stress in the bottom layer.

bottom and middle layers, while the stress on the top surface is still within the elastic limit. This is because the clamped ends and the pushing tool cause unbending, which leads to a tension on the bottom layer and a compression on the top layer. When the contact occurs between tool positions B and C, the sheet material is stretched and formed by the tool with a relatively small radius compared to the overall shape the deformed part has. Consequently, the metal is subjected to high through-thickness stress gradient at the punch tip, and the stress on the contacting surface (the bottom surface) was compressive in the minor stress on the sheet. After releasing the contact (or after the tool position D), stresses in all layers are unloaded.

Fig. 12(a) shows why the ISF enables the sheet metal to avoid a neck formation from the viewpoint that the initiation of any neck can be confirmed when all stresses through the sheet thickness exceed the limit. Before the contact with the tool, the top layer is subjected to a compression due to a springback of the sheet. Bending from the springback occurs in both the major and minor stress directions, which leads to the stable stress state on the top layer. The stresses on the top layer are always below the limit except during the time when the contact between the tool and the node occurs. Necking is suppressed due to bending caused by springback. During the contact, the stresses in all the layers have positive values in the major stress direction, because the tool and the clamped ends caused unbending which leads to a tension on all the layers. However, in the minor stress direction, the bottom surface is subjected to a compression. This is because a tool causes a local bending in the minor stress direction, while tensions caused by stretch-bending in the major direction dominate through all the layers. Because of the compression on the bottom surface, necking hardly initiates even though the contact occurs.

As the result shown in Fig. 12(a), the stress state for the top surface (the contact surface) is located inside the necking limit which

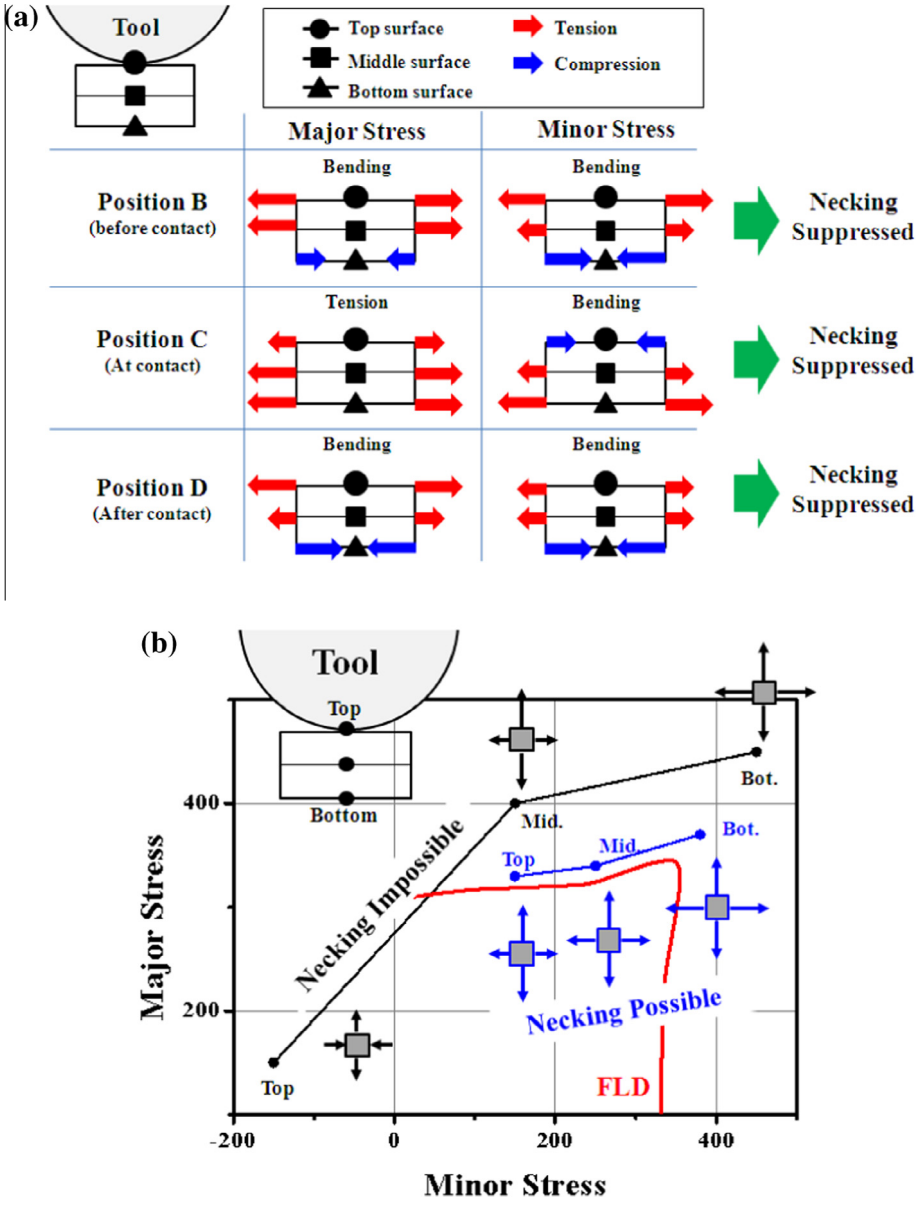

Fig. 12. Necking analysis based on stress gradient through the thickness direction.

delays the propagation of necking through the sheet thickness. A schematic view is shown in Fig. 12(b).

7. Conclusions

In this work, the stress-based FLC taking into account all the layers through the thickness direction was utilized to explain the reason why necking is suppressed in incremental sheet forming.

It was shown that the stresses and the strains exceed the forming limit diagrams in both strain and stress spaces when the information at the final state are used for the necking analysis. This result is contradictory to experimental observation. The stress histories of the node 1 which is a representative point for the plane strain deformation were presented in the FLCs. The stresses on the bottom and middle layers are repeatedly above the forming limit, while the stress on the top surface is always below the limit. Before the contact with the tool, the top surface is subjected to a compression due to the springback of the sheet. During the contact, the bottom surface is subjected to a compression in the minor stress direction, because a tool causes a local bending in the minor stress direction on the contacting part of the material. Attributed to these behaviors, all the stresses through the thickness direction did not exceed the stress-based forming limit at the same time. Initiation of any neck can be only confirmed when all stresses through the sheet thickness exceed the limit.

References

Dasappa, P., Inal, K., Mishra, R., 2012. The effects of anisotropic yield functions and their material parameters on prediction of forming limit diagrams. Int. J. Solids Struct. 49, 3528–3550.

Emmens, W.C., van den Boogaard, A.H., 2009. An overview of stabilizing deformation mechanisms in incremental sheet forming. J. Mater. Process. Technol. 209, 3688–3695.

Eyckens, P., He, S., Van Bael, A., Van Houtte, P., Duflou, J., 2007. Forming limit predictions for the serrated strain paths in single point incremental forming. In: Proceedings Numiform 07, Portugal, AIP CP908, 141–146.

Galerkin, B.G., 1915. Series solution of some problems in elastic equilibrium of rods and plates. Vestn. Inzh. Tech. 19, 897–908.

Guzmán, C.F., Gu, J., Duflou, J., Vanhove, H., Flores, P., Habraken, A.M., 2012. Study of the geometrical inaccuracy on a SPIF two-slope pyramid by finite element simulations. Int. J. Solids Struct. 49, 3594–3604.

Hencky, H., 1913. Der Spannungszustand in rechteckigen Platten (Ph.D. thesis). Darmstadt, Published by R. Oldenbourg, Munich and Berlin, Germany.
Hong, S.H., Yoon, J.W., Han, D.S., 2008. Anisotropic material modeling for automotive sheet alloys. NUMISHEET2008 edited by P. Hora, September 1–5, Interlaken, Switzerland, 105–110.
Love, A.E.H., 1927. A Treatise on the Mathematical Theory of Elasticity. Cambridge University Press, Cambridge, fourth edition.
MSC Software., 2010. Marc product documentation, Volume A: Theory and user information, 442–444.
Simha, C.H.M., Grantab, R., Worswick, M.J., 2007. Computational analysis of stress-based forming limit curves. Int. J. Solids Struct. 44, 8663–8684.
Stoughton, T.B., 2000. A general forming limit criterion for sheet metal forming. Int. J. Mech. Sci. 42, 1–27.
Stoughton, T.B., Zhu, X., 2004. Review of theoretical models of the strain-based FLD and their relevance to the stress-based FLD. Int. J. Plast. 20, 1463–1486.
Stoughton, T.B., Yoon, J.W., 2005. Sheet metal formability analysis for anisotropic materials under non-proportional loading. Int. J. Mech. Sci. 47, 1972–2002.
Stoughton, T.B., Yoon, J.W., 2011. A new approach for failure criterion for sheet metals. Int. J. Plast. 27, 440–459.
Stoughton, T.B., Yoon, J.W., 2012. Path independent forming limits in strain and stress spaces. Int. J. Solids Struct. 49, 3616–3625.
Tharrett, M., Stoughton, T., 2003. Stretch-bend forming limits of 1008 AK steel. SAE 2003–01-1157.
Timoshenko, S., Krieger, S.W., 1959. Theory of Plates and Shells, second edition. McGraw-Hill, New York.